

1 Controlling the Surface Hydroxyl Concentration by
2 Thermal Treatment of Layered Double Hydroxides

3 *Christopher M. R. Wright, Kanittika Ruengkajorn, Alexander F. R. Kilpatrick, Jean-Charles*
4 *Buffet and Dermot O'Hare**

5 Chemistry Research Laboratory, Department of Chemistry, University of Oxford, 12 Mansfield
6 Road, OX1 3TA, UK.

7

ABSTRACT

Layered double hydroxides (LDHs) are important materials in the field of catalyst supports and their surface hydroxyl functionality makes them interesting candidates for supporting of well-defined single-site catalysts. Here we report that the surface hydroxyl concentration can be controlled by thermal treatment of these materials under vacuum leading to hydroxyl numbers (α_{OH}) similar to that of dehydroxylated silica, alumina and magnesium hydroxide. Thermal treatment of $[\text{Mg}_{0.74}\text{Al}_{0.26}(\text{OH})_2](\text{SO}_4)_{0.1}(\text{CO}_3)_{0.03} \cdot 0.62(\text{H}_2\text{O}) \cdot 0.04(\text{acetone})$ prepared by the aqueous miscible organic solvent treatment method ($\text{Mg}_{2.84}\text{Al-SO}_4\text{-A AMO-LDH}$) is shown to yield a mixed metal oxide above 300 °C by a combination of thermogravimetric analysis (TGA) powder X-ray diffraction (PXRD), BET surface area analysis and FTIR spectroscopy. PXRD shows the disappearance of the characteristic LDH $00l$ peaks at 300 °C indicative of decomposition to the layered structure, coupled with a large increase in the BET surface area (95 vs 158 $\text{m}^2 \text{g}^{-1}$ from treatment at 275 and 300 °C respectively). Titration of the surface hydroxyls with $\text{Mg}(\text{CH}_2\text{Ph})_2(\text{THF})_2$ indicates that the hydroxyl number is independent of surface area for a given treatment temperature. Treatment at 450 °C under vacuum produces a mixed metal oxide material with a surface hydroxyl concentration (α_{OH}) of 2.14 OH nm^{-2} similar to the hydroxyl number (α_{OH}) of 1.80 OH nm^{-2} for a sample of SiO_2 dehydroxylated at 500 °C. These materials appear to be suitable candidates for use as single-site organometallic catalyst supports.

1 INTRODUCTION

2 For decades, heterogeneous catalysis has been widely utilized by industry for the production of
3 commodity chemicals, with silica commonly employed as the solid support.¹ For example, the
4 Phillips Triolefin Process for the metathesis of olefins, exploits a tungsten oxide catalyst
5 supported on silica to convert ethylene and butenes to propylene.^{2,3} Such processes allow for
6 facile product separation from the catalyst bed and in many cases permit the reactants to be
7 flowed. However, the supported species are ill-defined and hence the active species not fully
8 understood.⁴ Tailoring ligand design in homogeneous complexes has resulted in highly active
9 controllable catalysts.⁵ Traditional heterogeneous Ziegler-Natta olefin polymerization catalysts
10 (TiCl_4 supported on MgCl_2) have been partially replaced by metallocenes which display high
11 activity and allow for greater control of polymer properties.⁶ Recently, a new approach towards
12 heterogeneous catalyst design has emerged, this method known as Surface Organometallic
13 Chemistry (SOMC),^{7,8} takes these highly active well-defined catalysts and supports them on
14 solid oxides such as silica, alumina⁸ and zeolites.⁹ The idea is to view the surface hydroxyl
15 groups as ligands that can bind to the metal center of a complex displacing another ligand (*e.g.* a
16 methyl group to liberate methane). In order for this methodology to be successful only one
17 surface hydroxyl group should bind to the complex, and hence the distribution of the surface
18 hydroxyls needs to be controlled. This can be achieved by altering the dehydroxylation
19 temperature under vacuum, with higher temperatures yielding predominantly isolated sites that
20 are well separated. Work by Basset and co-workers demonstrated that when WMe_6 was
21 supported on dehydroxylated silica treated at 200 °C, both monopodal $\equiv\text{SiO-WMe}_5$ and bipodal
22 $(\equiv\text{SiO-})_2\text{WMe}_4$ formed due to the presence of vicinal silanols, whereas, when silica treated at
23 700 °C was used, only the monopodal species was observed.¹⁰

1 The nature of the immobilized complex is not the only factor that affects catalyst performance,
2 the support itself can also have a large influence on catalytic activity. Taoufik *et al.* investigated
3 the effect the dehydroxylation temperature of silica had on the activity of (n BuCp) $_2$ ZrCl $_2$
4 (Cp = cyclopentadienyl) supported on methylaluminoxane (MAO) coated silica. Their findings
5 demonstrated that there was an increase in the number of active sites with increasing
6 dehydroxylation temperature, however, the nature of these sites did not change.¹¹

7 Layered Double Hydroxides (LDHs) are a class of inorganic layered materials, consisting of
8 positively charged Brucite-like layers, bearing surface hydroxyl groups, with weakly bound
9 anions intercalated between them.¹² These highly tunable materials have been widely used for
10 catalysis,^{13,14} as their surfaces contain both acidic and basic sites which are altered by
11 calcination.¹⁵ Their main use in heterogeneous catalysis has been to support metallic species (*e.g.*
12 palladium nanoparticles for coupling reactions).^{16,17} The effect of thermal treatment on the
13 structural properties of LDHs is well understood, with removal of surface and interlayer water
14 observed at lower temperatures (below 200 °C), followed by dehydroxylation and loss of the
15 intercalated anions to yield Layered Double Oxide (LDO) materials, with further heating leading
16 to pure oxide phases.^{18,19} Despite this, study into the surface properties, in particular the surface
17 hydroxyl concentration as a function of treatment temperature is a relatively underexplored area.
18 Utilizing ^1H and ^{27}Al solid-state MAS NMR and FTIR spectroscopy, Peng and co-workers have
19 investigated the thermal decomposition of a series of MgAl-X LDHs (X = NO $_3$, CO $_3$, Cl and
20 ClO $_4$) with varying Mg:Al ratios.²⁰ In all cases, after dehydration (up to 150 °C),
21 dehydroxylation of Mg $_2$ AlOH groups and formation of four coordinate aluminum ions occurred
22 at lower temperatures than dehydroxylation of Mg $_3$ OH groups. At 375 °C, a reduction in the total

H content of 91.1% was observed by ^1H MAS solid-state NMR spectroscopy for $\text{Mg}_{0.73}\text{Al}_{0.27}(\text{OH})_2(\text{NO}_3)_{0.28}\cdot 0.62(\text{H}_2\text{O})$.

We have recently reported the synthesis of a new class of LDH materials by employing an Aqueous Miscible Organic Solvent Treatment (AMOST) method.^{21–23} These so called AMO-LDHs, have much higher surface areas than their conventionally synthesized counterparts and are easily dispersed in most organic solvents. AMO-LDHs can be represented by the general formula $[\text{M}^{2+}_{1-x}\text{M}^{3+}_x(\text{OH})_2]^{q+}(\text{X}^{n-})_{q/n}\cdot y(\text{H}_2\text{O})\cdot w(\text{AMO-solvent})$. Examples of M^{2+} include Mg^{2+} and Ca^{2+} , M^{3+} is usually Al^{3+} and X^{n-} may be a variety of anions such as Cl^- , NO_3^- , CO_3^{2-} and SO_4^{2-} and AMO-solvent is typically acetone or ethanol.

Amongst other applications, our group has looked at utilizing these materials as solid supports for catalysis, mainly ethylene polymerisation.^{24–28} Alterations in the composition have been shown to have a large effect on the activity of the supported species. Supporting of *rac*-EBIZrCl₂ (EBI = ethylenebis(indenyl)) on MAO coated AMO-LDHs ($[\text{M}^{2+}_{0.75}\text{M}^{3+}_{0.25}(\text{OH})_2](\text{X})_{0.25}\cdot y(\text{H}_2\text{O})\cdot w(\text{acetone})$; $\text{Ca}_3\text{Al-NO}_3$, $\text{Mg}_3\text{Ga-CO}_3$ and $\text{Mg}_3\text{Al-X}$, X = NO_3^- , Cl^- , SO_4^{2-} , CO_3^{2-} or borate) dehydroxylated at 150 °C led to catalysts that had a large variation in activity for ethylene polymerization, with $\text{Mg}_3\text{Al-SO}_4$ AMO-LDH shown to be the most active support ($5,613 \text{ kg}_{\text{PE}} \text{ mol}_{\text{Zr}}^{-1} \text{ h}^{-1}$).²⁵ This effect was also observed for supported tungsten imido complexes utilizing sulfate, nitrate and carbonate AMO-LDHs for the selective dimerisation of ethylene.²⁹ It was not possible in either case to explain this enhanced activity, thus warranting further investigation of the properties these materials exhibit after thermal treatment under vacuum.

Herein, we report the effect the dehydroxylation temperature has on the structural composition and degree of surface hydroxylation of high surface area

[Mg_{0.74}Al_{0.26}(OH)₂](SO₄)_{0.13}·0.71(H₂O)·0.17(acetone); Mg_{2.84}Al-SO₄-A AMO-LDH with a view to employing this material as a catalyst support using the SOMC methodology.

EXPERIMENTAL SECTION

General procedures

[Mg_{0.74}Al_{0.26}(OH)₂](SO₄)_{0.1}(CO₃)_{0.03}·0.62(H₂O)·0.04(acetone) (Mg_{2.84}Al-SO₄-A AMO-LDH) was commercially supplied by SCG Chemicals Co., Thailand, having been synthesized by a literature procedure²² and subsequently spray dried. [Mg_{0.64}Al_{0.36}(OH)₂](CO₃)_{0.18}·0.64(H₂O)·0.05(ethanol) (Mg_{1.71}Al-CO₃-E AMO-LDH) and [Mg_{0.74}Al_{0.26}(OH)₂](SO₄)_{0.13}·0.71(H₂O) (Mg_{2.83}Al-SO₄-W LDH) were synthesized according to literature procedures employing an initial Mg:Al ratio of 3:1.²² Elemental compositions (Mg and Al) were determined by ICP-MS analysis by Dr Alaa Abdul-Sada at the University of Sussex on an Agilent 7500 Series ICP-MS in helium collision mode. Samples (~20 mg) were digested in 10% nitric acid solution (10 mL) followed by a 100 fold dilution in dilute nitric acid. Analyses were run in triplicate against 5 standard concentrations and the data averaged (Tables S1-S3). Elemental analyses (C and H) were performed by Mr Stephen Boyer at London Metropolitan University (Table S4). Molarities of surface and interlayer water and AMO solvent were determined from the TGA analysis as these appear to be underestimated by the elemental analysis results. C₆D₆ (Sigma Aldrich) was dried over potassium under reflux, vacuum distilled and freeze-pump-thaw degassed three times before being stored in an MBraun Unilab glovebox prior to use. Si(SiMe₃)₄ (Sigma Aldrich) was stored in the glovebox prior to use. Mg(CH₂Ph)₂(THF)₂ was synthesized according to a literature procedure and stored in the glovebox prior to use.³⁰

Thermal vacuum treatment

LDH samples were thermally treated inside a quartz tube sealed at one end and connected to a vacuum/nitrogen manifold at the other, using a Carbolite HST 12/200 tube furnace. $\text{Mg}_{2.84}\text{Al-SO}_4\text{-A AMO-LDH}$ (~1 g) was loaded into a crucible and placed inside the tube. The sample was placed under dynamic vacuum (10^{-3} mbar) and the Carbolite 3216P1 temperature controller set to heat to the desired temperature at a ramp rate of $5\text{ }^\circ\text{C min}^{-1}$. Once at temperature it was held for 6 hours before cooling at a ramp rate of $10\text{ }^\circ\text{C min}^{-1}$, after which the samples were stored in a nitrogen filled glovebox. $\text{Mg}_{2.84}\text{Al-SO}_4\text{-A AMO-LDH}$ was dehydroxylated under vacuum over a range of temperatures (23, 100, 150, 200, 250, 275, 300, 350, 400 and $450\text{ }^\circ\text{C}$), $\text{Mg}_{1.77}\text{Al-CO}_3\text{-E AMO-LDH}$ and $\text{Mg}_{2.83}\text{Al-SO}_4\text{-W LDH}$ were dehydroxylated at $200\text{ }^\circ\text{C}$ for comparison. As the temperature of dehydroxylation was increased the initial white powder appeared greyer and darker which may be due to incomplete combustion of the AMO solvent.

Thermogravimetric (TGA) analysis

Thermogravimetric analyses were performed using a Mettler Toledo TGA/DSC 1 system. Samples (~10 mg) were quickly loaded from sealed vials into pre-tared alumina crucibles and placed under a flow of dry N_2 . The crucibles were heated from $25\text{--}600\text{ }^\circ\text{C}$ at a rate of $5\text{ }^\circ\text{C min}^{-1}$ under a flow of dry N_2 . Differential thermogravimetric analysis (DTG) is obtained from the 1st derivative of TGA data.

Powder X-ray diffraction (PXRD) analysis in capillary mode

PXRD samples were prepared in a glovebox by loading into capillary tubes which were then flame sealed. Samples were run utilizing a Siemens D5000 high-resolution X-ray powder diffractometer using $\text{Cu K}\alpha$ radiation ($\alpha_1 = 1.54057\text{ \AA}$, $\alpha_2 = 1.54433\text{ \AA}$, weighted average = 1.54178 \AA) after mounting on a goniometer. The capillaries were spun during

collection utilizing a mask of 20 mm, $1/8^\circ$ divergency, $1/8^\circ$ antiscatter, a fixed slit of $1/4^\circ$ at a step of 0.02° between 3 and 70° .

Infrared spectroscopy (FTIR)

FTIR samples were prepared in a glovebox using a specially designed press comprised of a metal holder into which two screws could be inserted at either end and tightened to form a pellet between them. Samples were ground with KBr and made into pellets, and the holder sealed between two KBr plates inside a metal casing. Spectra were recorded on a Nicolet iS5 ThermoScientific spectrometer in transmission mode (range $4000\text{--}400\text{ cm}^{-1}$, resolution 1 cm^{-1}).

Surface area and pore structure analysis

Specific surface areas (Brunauer-Emmett-Teller (BET) method) and pore volume (Barrett-Joyner-Halenda (BJH) method) were analyzed using a Micromeritics 3Flex Surface Characterization Analyzer. Samples ($\sim 100\text{ mg}$) were loaded in the glovebox into BET tubes and then sealed with a checkseal. The adsorption and desorption of N_2 at -196°C was then measured. Prior to each measurement samples were degassed at 30°C for 3 h.

NMR spectroscopy

Samples for NMR spectroscopy were made up in a glovebox, using 5 mm Young's tap NMR tubes. Spectra were recorded on a Bruker Avance III HD Nanobay 400 MHz NMR spectrometer and were referenced to the residual protio-solvent peak.

Surface hydroxyl titrations

In order to quantify the effect the dehydroxylation temperature has on the surface hydroxyl concentration titrations were undertaken using $\text{Mg}(\text{CH}_2\text{Ph})_2(\text{THF})_2$.³⁰ Reactions were carried out in duplicate for the AMO-LDH samples treated between 200 and 450°C in Young's NMR tubes. 5 mg of LDH and $\sim 10\text{ mg}$ $\text{Mg}(\text{CH}_2\text{Ph})_2(\text{THF})_2$ were mixed in 500 μL C_6D_6 containing

Si(SiMe₃)₄ as an internal standard ($c = 6.23 \text{ mmol dm}^{-3}$). Production of toluene resulting from protonation of the benzyl by the surface hydroxyls was monitored by ¹H NMR spectroscopy and the toluene methyl resonance integrated against that of Si(SiMe₃)₄.

Comparison of hydroxyl numbers with structurally characterized LDHs

The structures of brucite,³¹ hydrotalcite,³² quintinite³³ and LiAl₂(OD)₆Cl³⁴ were plotted using CrystalMaker software suite³⁵ from which a hydroxyl number (α_{OH}) could be determined by analysis of the unit cell contents. Pictorial representations of the dehydroxylated Mg_{2.84}Al-SO₄-A AMO-LDH surfaces were based on the hydrotalcite structure utilizing the hydroxyl numbers determined experimentally.

RESULTS AND DISCUSSION

Thermogravimetric analysis (TGA) of [Mg_{0.74}Al_{0.26}(OH)₂](SO₄)_{0.1}(CO₃)_{0.03}·0.62(H₂O)·0.04(acetone) (Mg_{2.84}Al-SO₄-A AMO-LDH) over a temperature range of 23-600 °C allows identification of the key steps in the thermal decomposition of LDHs. These are loss of coordinated surface and interlayer water and solvent molecules (50-200 °C, minimum in the 1st derivative labelled T₁), dehydroxylation of the surface hydroxyl groups leading to a layered double oxide (LDO) structure (200-400 °C, minimum labelled T₂), and further decomposition to mixed metal oxides.^{18,36} TGA of AMO-LDHs show that they exhibit lower minima for these decomposition events than their conventionally synthesized analogues. This difference has been attributed to a kinetic effect due to the better dispersion of the AMO-LDH particles,²² making the surface groups more accessible. The TGA trace for the untreated Mg_{2.84}Al-SO₄-A AMO-LDH is shown in Figure 1 and compared to those for Mg_{2.83}Al-SO₄-W LDH and Mg_{1.77}Al-CO₃-E AMO-LDH (Figure S1). For Mg_{2.84}Al-SO₄-A AMO-LDH the minima in the DTG for T₁ and T₂ occur at 142 and 394 °C respectively

(Figure S2 and Table S5). For the water washed sample ($\text{Mg}_{2.83}\text{Al-SO}_4\text{-W LDH}$) these events occur at much higher temperatures (192 and 408 °C, Figure S3) as has been observed previously.²² $\text{Mg}_{1.77}\text{Al-CO}_3\text{-E AMO-LDH}$ exhibits a similar T_1 of 140 °C to $\text{Mg}_{2.84}\text{Al-SO}_4\text{-A AMO-LDH}$, however the lower thermal stability of the intercalated carbonate leads to a much lower minimum for T_2 (336 °C vs 396 °C respectively, Figure S4 and Table S5). The total percentage mass lost at 500 °C is also much larger for $\text{Mg}_3\text{Al-CO}_3\text{ AMO-LDH}$ (42 vs 35%). This is due to decarboxylation and thus loss of the interlayer anion,³⁷ which occurs at lower temperatures than for the sulfate containing material.

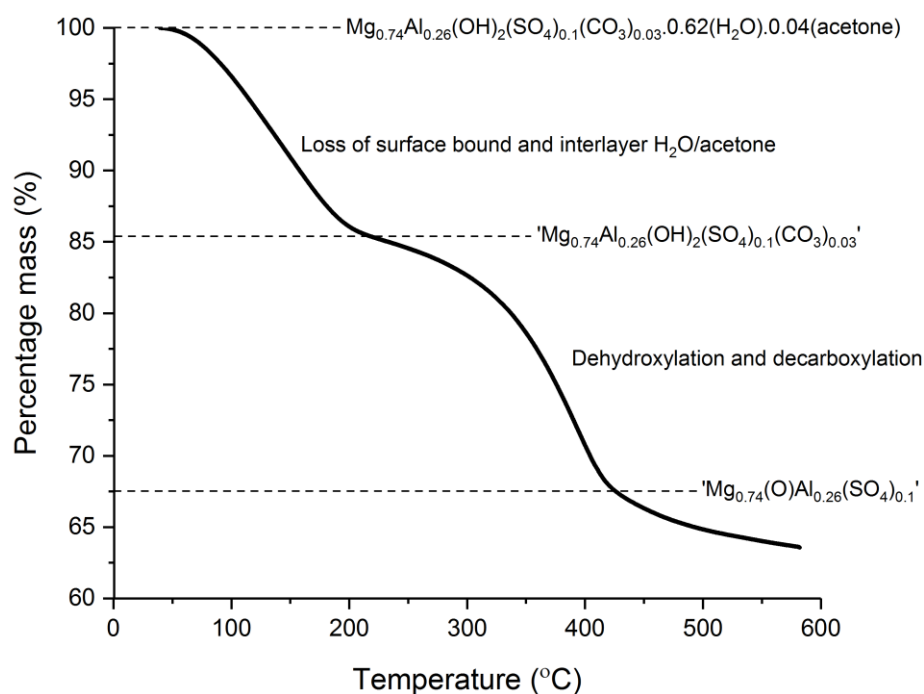


Figure 1. TGA of the $\text{Mg}_{2.84}\text{Al-SO}_4\text{-A AMO-LDH}$ starting material, displaying two clear steps attributed to loss of surface and interlayer water and acetone, and dehydroxylation respectively. Approximated molecular formulae are given at each step in the mass loss.

Comparison with the TGA data for $\text{Mg}_{2.32}\text{Al-SO}_4$ reported by Constantino *et al.*, further emphasizes the difference between conventionally synthesized and AMO-LDH materials. At 150 °C a percentage mass loss of ~9% is observed for the AMO-LDH compared to 3.4% for

$\text{Mg}_{2.32}\text{Al-SO}_4$,¹⁸ ascribed to the low boiling point and thus ease of removal of the AMO solvent. Theoretically, complete removal of surface and interlayer water and acetone from $[\text{Mg}_{0.74}\text{Al}_{0.26}(\text{OH})_2](\text{SO}_4)_{0.1}(\text{CO}_3)_{0.03} \cdot 0.62(\text{H}_2\text{O}) \cdot 0.04(\text{acetone})$ would result in a percentage mass loss of ~16% and formation of $[\text{Mg}_{0.74}\text{Al}_{0.26}(\text{OH})_2](\text{SO}_4)_{0.1}(\text{CO}_3)_{0.03}$, with further dehydration and decarboxylation to yield $[\text{Mg}_{0.75}\text{Al}_{0.25}(\text{O})](\text{SO}_4)_{0.1}$, resulting in a total percentage mass loss of 40%. As can be seen from the TGA the two observed steps correspond to percentage mass losses of 15 and 32%, hence we postulate that some hydroxyl groups persist even at temperatures >400 °C.

TGA analyses were performed on all of the $\text{Mg}_{2.84}\text{Al-SO}_4\text{-A}$ AMO-LDH compounds thermally treated under vacuum, which were compared with the starting AMO-LDH (Figure 2). Dry N_2 was employed to ensure that rehydration of the LDH structure did not occur. LDHs are known to exhibit a ‘memory effect’ having been calcined up to 450-600 °C, whereby, exposure to air leads to complete rehydration and restructuring of the LDH material.¹⁹ Individual TGA plots with DTG analysis are shown in the Supporting information (Figures S5–S13).

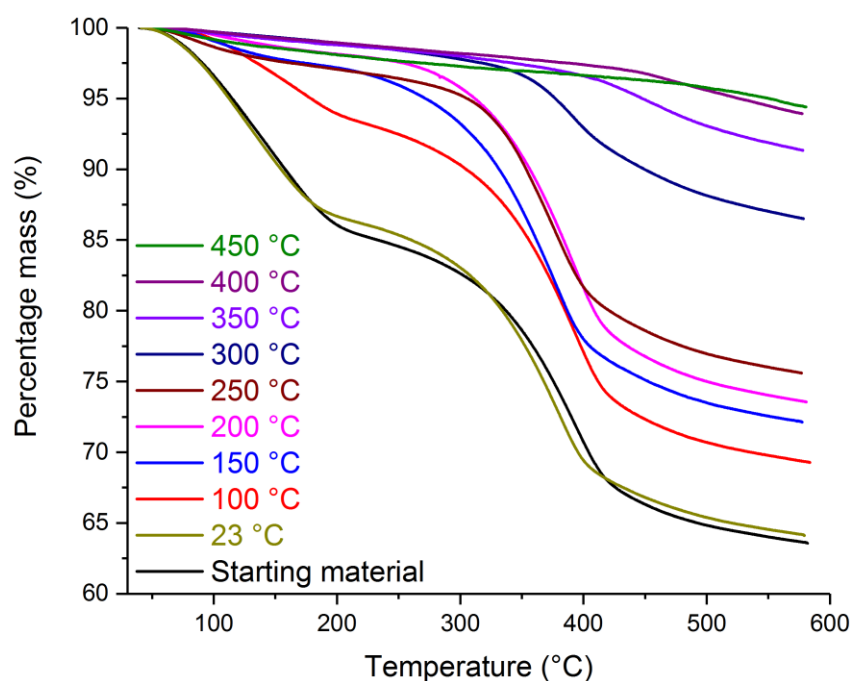


Figure 2. TGA analysis of thermally pre-treated $\text{Mg}_{2.84}\text{Al-SO}_4\text{-A AMO-LDH}$.

Analysis of the TGA curves for the dehydroxylated samples (Figure 2) shows that weight loss events only begin to occur at the temperature the material was treated at, as expected. For samples treated above 300 °C only a small decrease in the mass is observed, suggesting near complete dehydroxylation has occurred. Comparison of the sample evacuated at room temperature with the starting material shows that the end point for the first weight loss event transpires at a lower temperature, indicating that some of the surface bound water/solvent has been removed by such a process.

Powder X-ray diffraction (PXRD) patterns of the thermal treated LDHs were recorded in sealed capillaries under N_2 in transmission mode. The data in Figure 3 were collected over ~14 hours, the temperature dependence of the XRD data is tabulated in Table 1. The XRD of the starting $\text{Mg}_{2.84}\text{Al-SO}_4\text{-A AMO-LDH}$ may be indexed to a rhombohedral unit cell ($a = b = 3.06 \text{ \AA}$ and $c = 25.74 \text{ \AA}$). The Bragg reflections are consistent with a small platelet size, Scherrer analysis of the 003 Bragg peak width gives a crystalline length along the c-axis as 4.4 nm. On heating a shift in the 003 Bragg reflection to a higher 2θ was observed, signifying a decrease in the interlayer spacing calculated from the 003 peak position using the Bragg equation, with the peak widths (FWHM) remaining constant (Table 1).

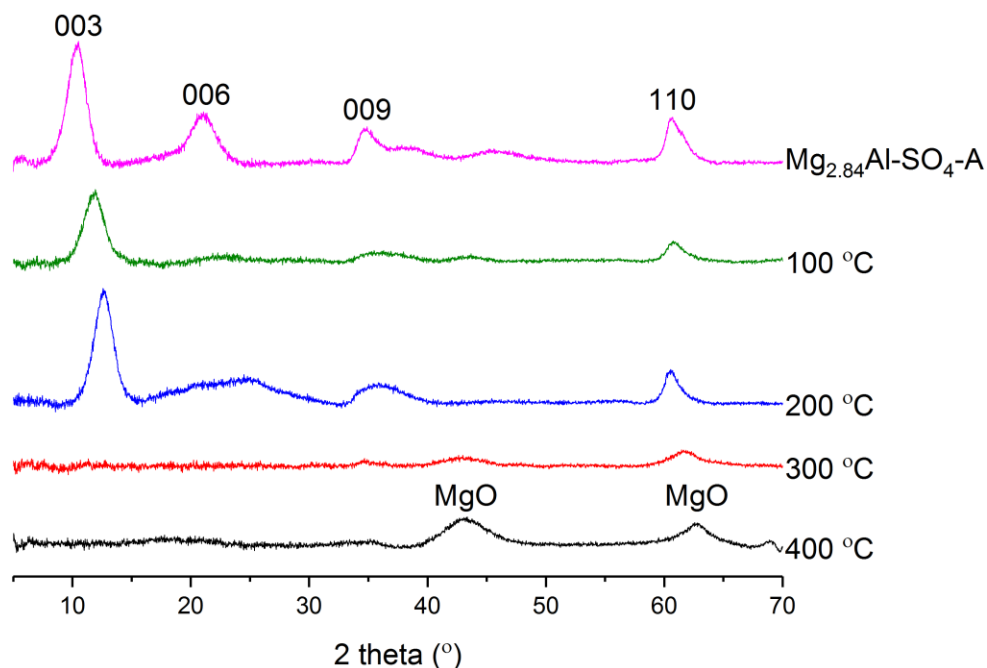


Figure 3. Transmission powder XRD patterns of the thermally treated $\text{Mg}_{2.84}\text{Al-SO}_4\text{-A}$ AMO-LDH samples at 100, 200, 300 and 400 °C.

Table 1. Comparison of the 003 Bragg peak position, full width half maximum (FWHM), and interlayer spacing and crystalline domain length for $\text{Mg}_{2.84}\text{Al-SO}_4\text{-A}$ AMO-LDH as a function of thermal treatment under vacuum at 100 and 200 °C.

Thermal treatment temp/°C	003 Bragg reflection/(2θ , °)	FWHM/(2θ , °)	Interlayer spacing/ (Å)	Crystalline Domain length /nm ^b
25	10.4 ^a	1.8	8.5	4.4
100	11.9	1.9	7.4	4.2
200	12.7	1.8	7.0	4.4

^a Indexed as rhombohedral unit cell $c = 3d(003) = 25.74$ Å; ^b using Scherrer equation, domain length = $(0.9 \times \lambda) / (\text{FWHM} \times \cos \theta)$.

Constantino *et al.* have attributed the reduction in the interlayer spacing seen for $\text{Mg}_{2.32}\text{Al-SO}_4$ calcined in air to sulfate grafting occurring between the layers.¹⁸ Above 300 °C, the 003 Bragg reflection is no longer observed indicating decomposition of a coherent layered structure has occurred. This broad almost featureless pattern is analogous to that observed when $\text{Mg}_{2.84}\text{Al-SO}_4\text{-A}$ LDH is calcined at 450 °C under a flow of nitrogen,¹⁸ again highlighting the

increased extent to which decomposition is observed with vacuum. A small shift in the 110 Bragg reflection is also observed between 200 and 300 °C ($2\theta = 60.6$ vs 61.4°) and hence a decrease in the a/b lattice parameters (Table S6). At 400 °C, formation of small amounts of MgO ($2\theta = 43.2$ and 62.7°) are observed, which correspond to a unit cell parameter $a = 4.19$ Å, smaller than that reported for the MgO rock salt structure ($a = 4.21$ Å) and is attributed to the presence of smaller Al^{3+} ions in an $\text{Mg}(\text{Al})\text{O}$ oxide structure, which has been observed previously.³⁸ The width of the MgO Bragg reflections is consistent with nanoparticle domain formation. A neutron diffraction study on the thermal decomposition of $\text{Mg}_{0.71}\text{Al}_{0.29}(\text{OH})_2(\text{CO}_3)_{0.145} \cdot m\text{H}_2\text{O}$ by Gazzano *et al.* also demonstrated a reduction in the interlayer spacing (c lattice parameter), with complete disappearance of the 003 Bragg reflection observed above 327 °C,³⁹ with an Mg–Al oxide structure similar to MgO identified. An increase in the a lattice parameter with temperature has also been observed which may indicate the removal of Al^{3+} ions from the oxide lattice.⁴⁰

FTIR spectroscopy of the samples shows a clear decrease in both the width and intensity of the OH stretches, which are associated with bound water molecules as well as surface and interlayer hydroxyl groups (Figure 4). A small amount of intercalated carbonate is also observed by the presence of the $\nu_3 \text{CO}_3$ stretch, which is most likely due to incomplete purging of the solvents and atmosphere during synthesis.

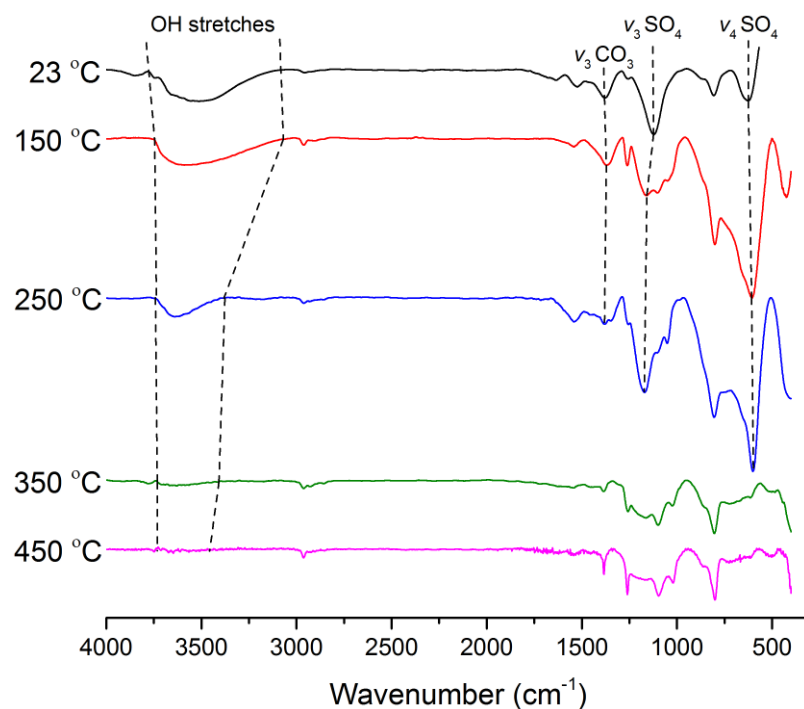


Figure 4. Comparison of the FTIR spectra for $\text{Mg}_{2.84}\text{Al-SO}_4\text{-A}$ AMO-LDH calcined at 23, 150, 250, 350 and 450 °C under vacuum.

There is a marked difference in the bands associated with the interlayer sulfate ions over the temperature range. The sulfate molecules are proposed to have restricted rotation within the gallery, with the symmetrical ν_3 band for tetrahedral sulfate, observed at 1121 cm^{-1} for the 23 °C sample, split at higher temperatures due to a lowering symmetry in the intercalate.¹⁸ The band at 1100 cm^{-1} appears to shift to slightly higher wavenumbers over the temperature range 23–250 °C (Table S7); the splitting of this band is indicative of sulfate grafting to the internal LDH surface,¹⁸ supporting the observed decrease in the c dimension from the PXRD. Above this temperature, the relative intensity of these bands is markedly reduced, suggesting loss of interlayer sulfate ions due to formation of metal oxide salts.

By focusing on the hydroxyl region ($3000\text{--}4000\text{ cm}^{-1}$) (Figure 5), a reduction in both the width and intensity of the bands is clearly observed as the temperature is increased. Three groups of similar width and intensity are observed (23-150, 200-300 and 350 to 450 °C) matching the mass

loss events in the TGA. There is a clear shift in the minimum between 23 and 300 °C towards higher wavenumbers (3512 vs 3649 cm^{-1}) (Table S7). Between 200 and 300 °C, the loss of surface water and concomitant dehydroxylation yields bands with approximately half the area of the samples treated at lower temperatures. Above 300 °C, near complete dehydroxylation is seen to occur with only very weak stretches between 3400–3700 cm^{-1} present. The observed hydroxyl bands are not as narrow as those observed for dehydroxylated silica samples⁴¹ due to the presence of internal hydroxyl groups within the layers.

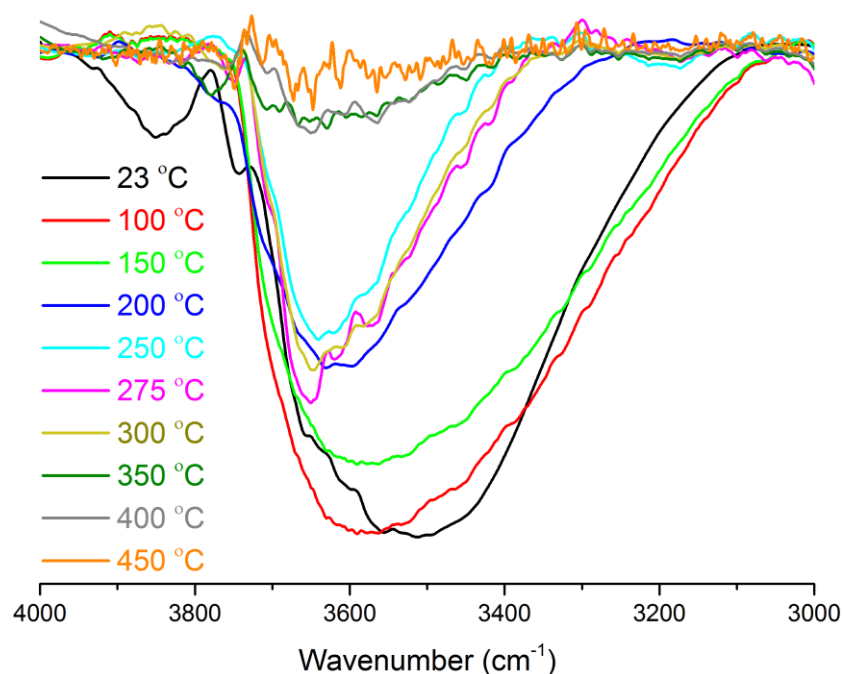


Figure 5. Comparison of the OH region of the FTIR spectrum (3000–3800 cm^{-1}) for $\text{Mg}_{2.84}\text{Al-SO}_4\text{-A}$ AMO-LDH thermally treated between 23–450 °C under vacuum.

The specific surface area of the AMO-LDH samples were determined by N_2 gas physisorption using Brunauer-Emmett-Teller (BET) theory, which revealed that the surface area of the samples increases with increasing dehydroxylation temperature (Figure 6). There appear to be two regimes, one below 275 °C where the surface area gradually increases and one above 300 °C where it increases linearly at a higher rate, with a large jump between them (95 to 158 m^2g^{-1}

respectively), further demonstrating the structural change occurring in this material. Complete erosion of the layered structure would yield single layer mixed metal oxide sheets, thus increasing the surface area. Bellotto *et al.* have also previously observed a large increase in the surface area of calcined $[\text{Mg}_{0.64}\text{Al}_{0.36}(\text{OH})_2](\text{CO}_3)_{0.18} \cdot 0.46\text{H}_2\text{O}$ after loss of the layered structure is observed.⁴²

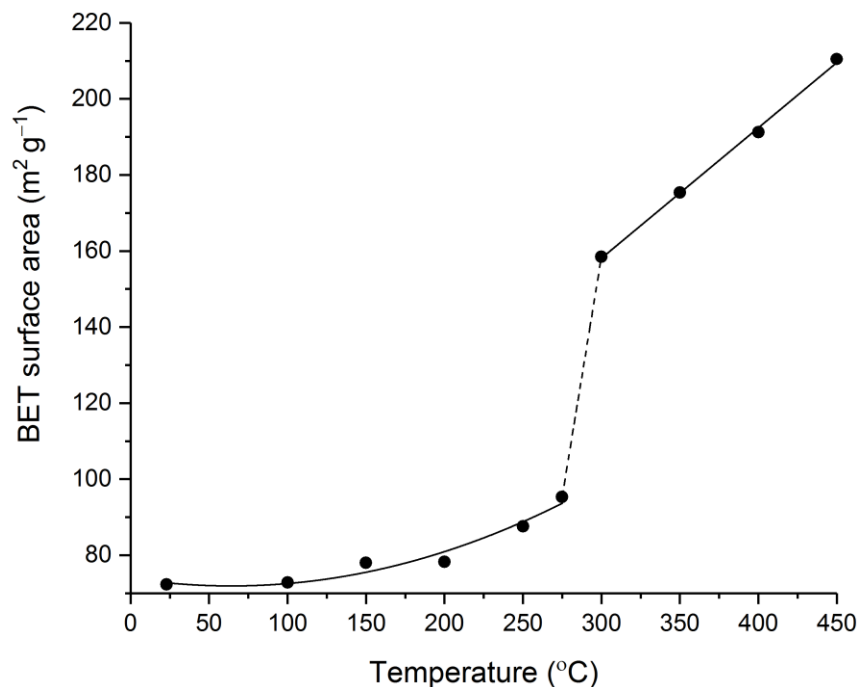


Figure 6. BET surface area measurements for $\text{Mg}_{2.84}\text{Al-SO}_4\text{-A}$ AMO-LDH samples thermally treated between 23 and 450 °C. Trend lines are a guide for the eye.

BET and pore volume data (Table S8) along with individual BET isotherms and pore volume distributions are provided in the Supporting Information (Figures S14–S33). The isotherms follow classical type II and type IV shapes indicating that the material is mesoporous.⁴³ At higher temperatures, the total pore volume increases (calculated by the Barrett-Joyner-Halenda (BJH) method), with a greater H3 hysteresis loop (Figure 7) indicating that there are additional cylindrical pores occurring between aggregated LDH platelet shaped particles.^{43,44} From the pore volume distributions an increase in mesopores of size ranging between 30–50 Å is observed

(4.4% of total pores in the starting material vs 27% at 450 °C) (Table S8). The most notable increase in pores of this size occurs between 275 and 300 °C, where it doubles from 8 to 16% of the total. This is also the temperature range where loss of the layered structure and increase in the surface area are observed.

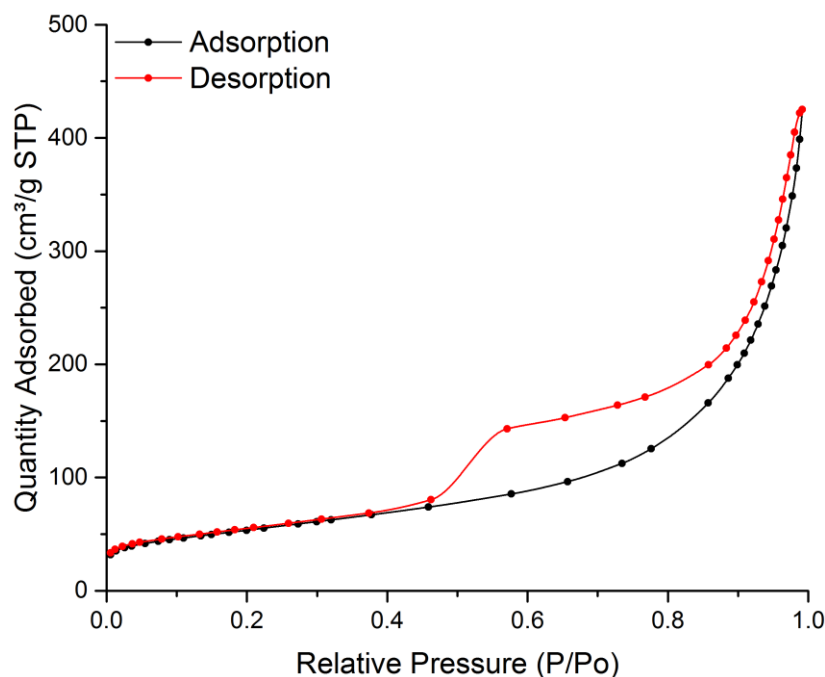


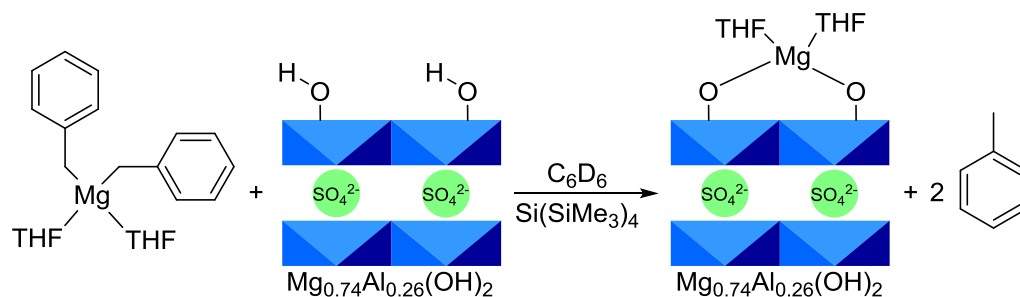
Figure 7. BET adsorption and desorption isotherms for $\text{Mg}_{2.84}\text{Al-SO}_4\text{-A}$ AMO-LDH thermally treated at 400 °C under vacuum displaying a H3 type hysteresis.

Comparison of the BET surface area of $\text{Mg}_{2.84}\text{Al-SO}_4\text{-A}$ AMO-LDH with $\text{Mg}_{1.71}\text{Al-CO}_3\text{-E}$ AMO-LDH and $\text{Mg}_{2.83}\text{Al-SO}_4\text{-W}$ LDH all thermally treated under vacuum at 200 °C (Table S8) shows a marked increase for those exposed to the AMO treatment (77 and 313 vs 12 $\text{m}^2 \text{g}^{-1}$ respectively).

The concentration of surface silanols at a given temperature has been well determined for dehydroxylated silica.^{45–47} Techniques have been developed in order to measure the type and number of surface hydroxyl groups on metal oxides, such as IR,^{45,48} TGA,⁴⁹ solid-state NMR⁵⁰ and deuterium exchange.⁴⁸ One of the simplest methods is to titrate the surface hydroxyl groups

using organometallic reagents.^{51,52} Reaction of surface hydroxyl groups with $\text{Mg}(\text{CH}_2\text{Ph})_2(\text{THF})_2$ ³⁰ liberates toluene that can be integrated against an internal standard (Scheme 1). Reactions were carried out in Young's NMR tubes with 5 mg LDH and ~10 mg $\text{Mg}(\text{CH}_2\text{Ph})_2(\text{THF})_2$ in C_6D_6 containing a known concentration of $\text{Si}(\text{SiMe}_3)_4$ as the internal standard (Figure S38).

Scheme 1. Schematic representation showing the titration of $\text{Mg}_{2.84}\text{Al-SO}_4\text{-A AMO-LDH}$ with $\text{Mg}(\text{CH}_2\text{Ph})_2(\text{THF})_2$.



From the data obtained, the molar equivalents of hydroxyls per gram of solid can be calculated and the hydroxyl number, α_{OH} , for each sample determined utilizing the surface areas determined from the BET analysis (Figure 8 and Table S21). The hydroxyl number refers to the concentration of surface hydroxyls, given as the number of OH groups per square nanometer (OH nm^{-2}). As the treatment temperature is increased the degree of surface hydroxylation falls following an exponential decay type pattern, from 13.4 to 2.1 OH nm^{-2} over the range 200–450 °C.

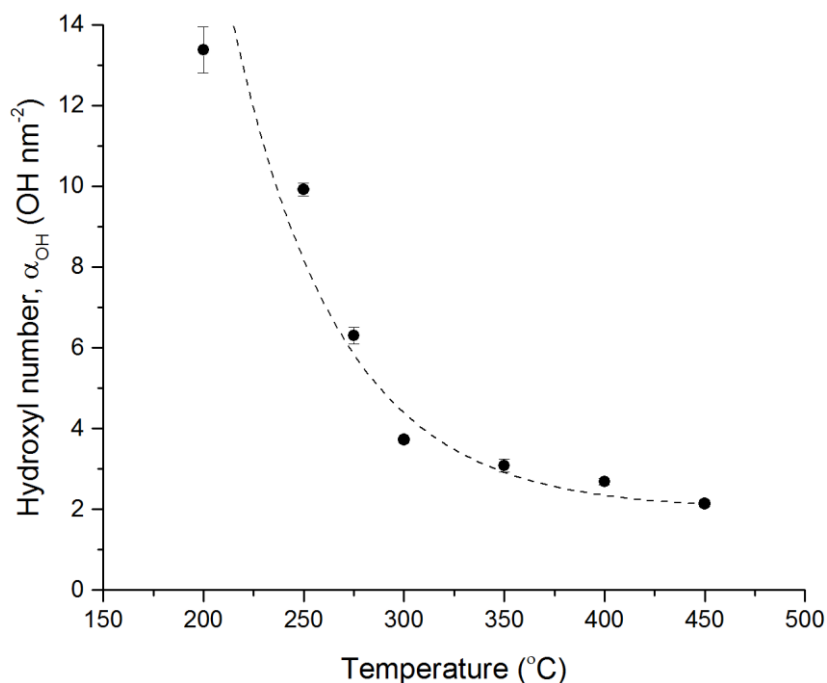


Figure 8. Hydroxyl number (α_{OH}) determined from titration and BET data as a function of the thermal treatment temperature for $Mg_{2.84}Al-SO_4-A$ AMO-LDH.

The hydroxyl numbers (α_{OH}) for $Mg_{1.77}Al-CO_3-E$ AMO-LDH and $Mg_{2.83}Al-SO_4-W$ LDH both thermally treated at 200 °C under vacuum are calculated as being 14.0 and 14.2 OH nm⁻², which are close to that of the analogously treated sulfate sample (13.4 OH nm⁻²) (Table S21). From this result we can infer that both variation in the interlayer anion, or surface area of the AMO-LDH have little effect on the degree of dehydroxylation of the surface. Zhuravlev and co-workers have previously shown that the α_{OH} of amorphous silicas are independent of the specific surface area for a given temperature of treatment. This is due to the linear dependence of the surface area with the hydroxyl density (mol_{OH} g⁻¹).⁴⁵ Whilst the hydroxyl number is independent of the surface area, there is a large difference in the number moles of hydroxyl per gram of solid between the AMO treated $Mg_{1.77}Al-CO_3-E$ and water washed $Mg_{2.83}Al-SO_4-W$ LDHs (7.29 vs 0.28 mmol_{OH} g⁻¹). For catalytic applications, this increased number of accessible hydroxyls, should allow for increased complex loadings when compared to the conventional LDH. The hydroxyl number

1 calculated for $\text{Mg}_{2.84}\text{Al-SO}_4\text{-A AMO-LDH}$ at 450 °C (2.1 OH nm^{-2}) can be compared with
2 values determined for silica,⁴⁵ alumina⁵³ and magnesium oxide⁵⁴ all treated at 500 °C (1.8, 2.7
3 and 3.6 OH nm^{-2} respectively, Table S21) and is seen to mirror that of silica falling below those
4 of alumina and MgO.

5 To further corroborate the results, hydroxyl numbers were determined from the reported
6 structures obtained by combined neutron and powder X-ray diffraction refinement for brucite,³¹
7 hydroxalcite,³² quintinite³³ and $\text{LiAl}_2(\text{OH})_6\text{Cl}$,³⁴ the latter determined after calcination at 90 °C,
8 and compared to those measured experimentally for $\text{Mg}_{2.84}\text{Al-SO}_4\text{-A AMO-LDH}$ (Table 2). This
9 was achieved by calculating the number of hydroxyl groups inside the unit cell and dividing the
10 number by the unit cell surface area. An example calculation is given for $\text{LiAl}_2(\text{OH})_6\text{Cl}$ in the
11 ESI (Equation S1).

12 The hydroxyl numbers are all slightly below the value obtained experimentally for
13 $\text{Mg}_{2.84}\text{Al-SO}_4\text{-A AMO-LDH}$ dehydroxylated at 200 °C. One reason for this may be that there are
14 no water molecules included in the structural fittings as they have been assumed to be removed
15 after thermal treatment. Our results indicate at least for the $\text{Mg}_{2.84}\text{Al-SO}_4\text{-A AMO-LDH}$ used in
16 our study that this does not occur until temperatures above ~150 °C.

17 By utilizing the hydroxyl numbers determined experimentally and assuming a uniform
18 dispersion of the remaining hydroxyls after thermal treatment under vacuum, an approximate
19 OH–OH proximity can be calculated. Each OH site is proposed to occupy a spherical surface
20 area of radius r , whereby neighboring hydroxyls are a distance of $2r$ apart. As the number of
21 these hydroxyls that occupy 1 nm^2 has been determined experimentally the area occupied by
22 each hydroxyl can be calculated and r determined. Such a treatment for $\text{Mg}_{2.84}\text{Al-SO}_4\text{-A}$

1 AMO-LDH treated at 200, 300 and 450 °C yields OH–OH proximities of 3, 6 and 8 Å
 2 respectively.

3 **Table 2.** Surface hydroxyl numbers and proximities for the dehydroxylated AMO-LDH samples
 4 with values calculated for similar structurally characterized materials.

LDH Sample / dehydroxylation temperature (°C)	Hydroxyl number, α_{OH} (OH nm ⁻²)	OH–OH proximity (Å)
Brucite [Mg(OD) ₂] / n/a ³¹	11.7*	3
Hydrotalcite [Mg ₆ Al ₂ (OH) ₁₆ (CO ₃)(H ₂ O) ₄] / n/a ³²	12.4*	3
Quintinite [Mg ₄ Al ₂ (OH) ₁₂ (CO ₃)(H ₂ O) ₃] / n/a ³³	12.5*	3
LiAl ₂ (OH) ₆ Cl / 90 ³⁴	13.3*	3
Mg _{2.84} Al-SO ₄ -A / 200	13.4 ± 0.56	3
Mg _{2.84} Al-SO ₄ -A / 300	3.7 ± 0.07	6
Mg _{2.84} Al-SO ₄ -A / 450	2.1 ± 0.08	8

5 * Determined from the combined powder X-ray and neutron diffraction refinement.

6 By systematic removal of OH groups assuming a uniform hydroxyl distribution the
 7 experimentally determined α_{OH} values can be pictorially represented using the surface of the
 8 hydrotalcite structure (previously determined by neutron diffraction³²) having calculated the unit
 9 cell surface area (Figure 9). Due to the loss of layered structure above 300 °C, these are shown as
 10 mixed metal oxide sheets. Measurements of the OH proximities from these depictions are in
 11 good agreement with the values determined using the experimental data.

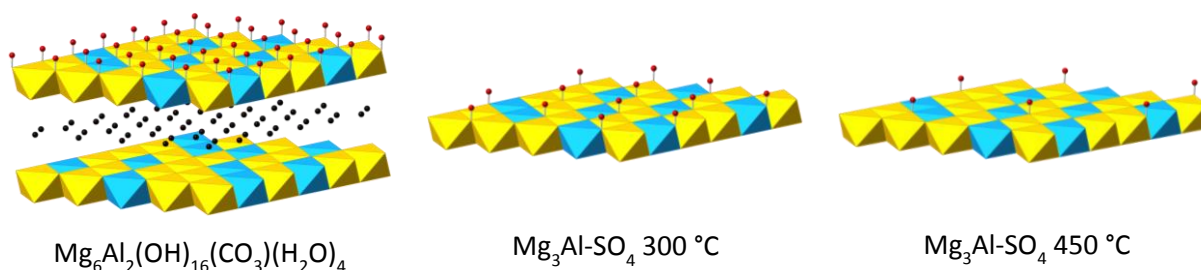


Figure 9. Surface hydroxyl concentration of hydrotalcite $[\text{Mg}_6\text{Al}_2(\text{OH})_{16}(\text{CO}_3)(\text{H}_2\text{O})_4]$ (neutron diffraction),³² a pictorial depiction of $\text{Mg}_{2.84}\text{Al-SO}_4\text{-A}$ AMO-LDH dehydroxylated at 300 °C and 450 °C utilizing the calculated hydroxyl numbers (α_{OH}).

We have previously reported the use of thermally treated AMO-LDHs as supports for metallocene pre-catalysts for ethylene polymerization after initial coating of the LDH surface with methylaluminoxane (MAO). Analysis of the activity based on the temperature of thermal treatment under vacuum for $\text{MgAl-CO}_3\text{-A}$ AMO-LDH with *rac*-EBIZrCl₂ over the range 0–200 °C showed that peak activity was observed at 150 °C.²⁴ From our results it is above this temperature that surface hydroxyls begin to be removed which may yield more Lewis acidic sites, which is a proposed reason for deactivation of $(^n\text{BuCp})_2\text{ZrCl}_2$ immobilized on MAO coated silica-alumina at higher calcination temperatures.⁵⁵ Below temperatures of 150 °C surface water will hydrolyze the MAO reducing its performance as an activator. As mentioned previously, sulfate intercalated AMO-LDHs have been shown to outperform other anions when employed as catalyst supports.^{25,29} From the data obtained in this study comparing sulfate and carbonate containing LDHs, very little difference is observed in the surface hydroxyl concentrations. However despite analogous synthetic procedures employing an initial Mg:Al of 3:1, the ratio for the carbonate AMO-LDH is much lower than for the sulfate (1.77 vs 2.84) and may be the reason behind the reduced activities, warranting further study in this area.

CONCLUSIONS

$\text{Mg}_{2.84}\text{Al-SO}_4\text{-A}$ AMO-LDH was treated at various temperatures under vacuum and compared to $\text{Mg}_{1.77}\text{Al-CO}_3\text{-E}$ AMO-LDH and $\text{Mg}_{2.83}\text{Al-SO}_4\text{-W}$ LDH both treated at 200 °C. A significant structural change is observed at 300 °C by powder XRD with a loss of the layered arrangement, coupled to a large increase in the BET surface area. A large decrease in the surface hydroxyl concentration of these materials is observed by NMR spectroscopic titrations and infrared

spectroscopy. The hydroxyl numbers calculated appear to be independent of the surface area and intercalated anion at a given treatment temperature. The hydroxyl numbers calculated for $\text{Mg}_{2.84}\text{Al-SO}_4\text{-A}$ treated above 300 °C are shown to be in the range of other defined support materials. These materials can now be tested as supports for well-defined air and moisture sensitive organometallic complexes utilizing the SOMC methodology for use in organic transformations, which is currently under investigation.

ASSOCIATED CONTENT

The following files are available free of charge.

Electronic Supplementary Information (ESI): Additional characterizing data (Individual TGA and DTG analysis and data table, table of FTIR peak shifts, table of XRD peak shifts, BET isotherms and pore volume distributions and data table, surface hydroxyl calculations from refined structures and example NMR titration data) (PDF).

AUTHOR INFORMATION

Corresponding Author

*dermot.ohare@chem.ox.ac.uk

Author Contributions

The manuscript was written through contributions of all authors. All authors have given approval to the final version of the manuscript.

Funding Sources

This work was supported by the Engineering and Physical Sciences Research Council (U.K.) (EP/L50503/1). We also thank SCG Packaging Co. Ltd, Thailand for a graduate scholarship

1 (KR), Wadham College Oxford for a RJP Williams JRF (AFRK) and SCG Chemicals Co. Ltd,
2 Thailand for funding (AFRK and J-CB).

3 **ACKNOWLEDGMENT**

4 The authors would like to thank the surface analysis facility, University of Oxford, for use of the
5 TGA and BET machines and Mr Phakpoom Angpanitcharoen (University of Oxford) for SEM
6 images.

7 **ABBREVIATIONS**

8 LDH, Layered Double Hydroxide; AMO, Aqueous Miscible Organic solvent treated; TGA
9 Thermogravimetric Analysis; PXRD, Powder X-Ray Diffraction; FWHM, Full Width Half
10 Maximum; FTIR, Fourier Transform Infrared; BET, Brunauer-Emmett-Teller; BJH, Barrett-
11 Joyner-Halenda; SEM, Scanning Electron Microscopy; NMR, Nuclear Magnetic Resonance.

12

1 REFERENCES

- 2 (1) Joshi, S. S.; Ranade, V. V. *Industrial Catalytic Processes for Fine and Specialty*
3 *Chemicals*; Joshi, S. S., Ranade, V. V., Eds.; Elsevier, 2016.
- 4 (2) Heckelsberg, L. F.; Banks, R. L.; Bailey, G. C. A Tungsten Oxide on Silica Catalyst for
5 Phillips' Triolefin Process. *Ind. Eng. Chem. Prod. Res. Dev.* **1968**, 7, 29–31.
- 6 (3) Mol, J. Industrial Applications of Olefin Metathesis. *J. Mol. Catal. A Chem.* **2004**, 213
7 (1), 39–45.
- 8 (4) Copéret, C. Molecular Design of Heterogeneous Catalysts: The Case of Olefin Metathesis.
9 *New J. Chem.* **2004**, 28, 1–10.
- 10 (5) Dewaele, A.; Verpoort, F.; Sels, B. Opportunities of Immobilized Homogeneous
11 Metathesis Complexes as Prominent Heterogeneous Catalysts. *ChemCatChem* **2016**, 8,
12 3010–3030.
- 13 (6) Shamiri, A.; Chakrabarti, M.; Jahan, S.; Hussain, M.; Kaminsky, W.; Aravind, P.; Yehye,
14 W. The Influence of Ziegler-Natta and Metallocene Catalysts on Polyolefin Structure,
15 Properties, and Processing Ability. *Materials* **2014**, 7, 5069–5108.
- 16 (7) *Modern Surface Organometallic Chemistry*; Basset, J.-M., Psaro, R., Roberto, D., Ugo,
17 R., Eds.; Wiley-VCH Verlag GmbH & Co. KGaA: Weinheim, Germany, 2009.
- 18 (8) Copéret, C.; Comas-Vives, A.; Conley, M. P.; Estes, D. P.; Fedorov, A.; Mougel, V.;
19 Nagae, H.; Núñez-Zarur, F.; Zhizhko, P. A. Surface Organometallic and Coordination
20 Chemistry toward Single-Site Heterogeneous Catalysts: Strategies, Methods, Structures,
21 and Activities. *Chem. Rev.* **2016**, 116, 323–421.

- 1 (9) Guzman, J.; Gates, B. C. Supported Molecular Catalysts: Metal Complexes and Clusters
2 on Oxides and Zeolites. *Dalton Trans.* **2003**, *17*, 3303–3318.
- 3 (10) Samantaray, M. K.; Callens, E.; Abou-Hamad, E.; Rossini, A. J.; Widdifield, C. M.; Dey,
4 R.; Emsley, L.; Basset, J.-M. WMe₆ Tamed by Silica: ≡Si–O–WMe₅ as an Efficient, Well-
5 Defined Species for Alkane Metathesis, Leading to the Observation of a Supported W–
6 Methyl/Methylidyne Species. *J. Am. Chem. Soc.* **2014**, *136*, 1054–1061.
- 7 (11) Bashir, M. A.; Vancompernelle, T.; Gauvin, R. M.; Delevoye, L.; Merle, N.; Monteil, V.;
8 Taoufik, M.; McKenna, T. F. L.; Boisson, C. Silica/MAO/(*n*-BuCp)₂ZrCl₂ Catalyst: Effect
9 of Support Dehydroxylation Temperature on the Grafting of MAO and Ethylene
10 Polymerization. *Catal. Sci. Technol.* **2016**, *6*, 2962–2974.
- 11 (12) Zhang, J.; Zhang, F.; Ren, L.; Evans, D. G.; Duan, X. Synthesis of Layered Double
12 Hydroxide Anionic Clays Intercalated by Carboxylate Anions. *Mater. Chem. Phys.* **2004**,
13 *85*, 207–214.
- 14 (13) Fan, G.; Li, F.; Evans, D. G.; Duan, X. Catalytic Applications of Layered Double
15 Hydroxides: Recent Advances and Perspectives. *Chem. Soc. Rev.* **2014**, *43*, 7040–7066.
- 16 (14) Xu, Z. P.; Zhang, J.; Adebajo, M. O.; Zhang, H.; Zhou, C. Catalytic Applications of
17 Layered Double Hydroxides and Derivatives. *Appl. Clay Sci.* **2011**, *53*, 139–150.
- 18 (15) Kagunya, W.; Hassan, Z.; Jones, W. Catalytic Properties of Layered Double Hydroxides
19 and Their Calcined Derivatives. *Inorg. Chem.* **1996**, *35*, 5970–5974.
- 20 (16) Choudary, B. M.; Madhi, S.; Chowdari, N. S.; Kantam, M. L.; Sreedhar, B. Layered
21 Double Hydroxide Supported Nanopalladium Catalyst for Heck-, Suzuki-, Sonogashira-,

- 1 and Stille-Type Coupling Reactions of Chloroarenes. *J. Am. Chem. Soc.* **2002**, *124*,
2 14127–14136.
- 3 (17) Takehira, K. Recent Development of Layered Double Hydroxide-Derived Catalysts
4 – Rehydration, Reconstitution, and Supporting, Aiming at Commercial Application –.
5 *Appl. Clay Sci.* **2017**, *136*, 112–141.
- 6 (18) Constantino, V. R. L.; Pinnavaia, T. J. Basic Properties of $\text{Mg}^{2+}_{1-x}\text{Al}^{3+}_x$ Layered Double
7 Hydroxides Intercalated by Carbonate, Hydroxide, Chloride, and Sulfate Anions. *Inorg.*
8 *Chem.* **1995**, *34*, 883–892.
- 9 (19) Cavani, F.; Trifirò, F.; Vaccari, A. Hydrotalcite-Type Anionic Clays: Preparation,
10 Properties and Applications. *Catal. Today* **1991**, *11*, 173–301.
- 11 (20) Yu, G.; Zhou, Y.; Yang, R.; Wang, M.; Shen, L.; Li, Y.; Xue, N.; Guo, X.; Ding, W.;
12 Peng, L. Dehydration and Dehydroxylation of Layered Double Hydroxides: New Insights
13 from Solid-State NMR and FT-IR Studies of Deuterated Samples. *J. Phys. Chem. C* **2015**,
14 *119*, 12325–12334.
- 15 (21) Wang, Q.; O'Hare, D. Large-Scale Synthesis of Highly Dispersed Layered Double
16 Hydroxide Powders Containing Delaminated Single Layer Nanosheets. *Chem. Comm.*
17 **2013**, *49*, 6301–6303.
- 18 (22) Chen, C.; Yang, M.; Wang, Q.; Buffet, J.-C.; O'Hare, D. Synthesis and Characterisation
19 of Aqueous Miscible Organic-Layered Double Hydroxides. *J. Mater. Chem. A* **2014**, *2*,
20 15102–15110.
- 21 (23) Chen, C.; Wangriya, A.; Buffet, J.-C.; O'Hare, D. Tuneable Ultra High Specific Surface

- Area Mg/Al-CO₃ Layered Double Hydroxides. *Dalton Trans.* **2015**, 44, 16392–16398.
- (24) Buffet, J.-C.; Turner, Z. R.; Cooper, R. T.; O'Hare, D. Ethylene Polymerisation Using Solid Catalysts Based on Layered Double Hydroxides. *Polym. Chem.* **2015**, 6, 2493–2503.
- (25) Buffet, J.-C.; Wana, N.; Arnold, T. A. Q.; Gibson, E. K.; Wells, P. P.; Wang, Q.; Tantirungrotechai, J.; O'Hare, D. Highly Tunable Catalyst Supports for Single-Site Ethylene Polymerization. *Chem. Mater.* **2015**, 27, 1495–1501.
- (26) Buffet, J.-C.; Arnold, T. A. Q.; Turner, Z. R.; Angpanitcharoen, P.; O'Hare, D. Synthesis and Characterisation of Permethylindenyl Zirconium Complexes and Their Use in Ethylene Polymerisation. *RSC Adv.* **2015**, 5, 87456–87464.
- (27) Fraser, D. A. X.; Turner, Z. R.; Buffet, J.-C.; O'Hare, D. Titanium and Zirconium Permethylpentalene Complexes, Pn*MCpRX, as Ethylene Polymerization Catalysts. *Organometallics* **2016**, 35, 2664–2674.
- (28) Buffet, J.-C.; Byles, C. F. H.; Felton, R.; Chen, C.; O'Hare, D. Metallocene Supported core@LDH Catalysts for Slurry Phase Ethylene Polymerisation. *Chem. Commun.* **2016**, 52, 4076–4079.
- (29) Wright, C. M. R.; Turner, Z. R.; Buffet, J.-C.; O'Hare, D. Tungsten Imido Catalysts for Selective Ethylene Dimerisation. *Chem. Commun.* **2016**, 52, 2850–2853.
- (30) Bailey, P. J.; Coxall, R. A.; Dick, C. M.; Fabre, S.; Henderson, L. C.; Herber, C.; Liddle, S. T.; Loroño-González, D.; Parkin, A.; Parsons, S. The First Structural Characterisation of a Group 2 Metal Alkylperoxide Complex: Comments on the Cleavage of Dioxygen by Magnesium Alkyl Complexes. *Chem. Eur. J.* **2003**, 9, 4820–4828.

- 1 (31) Parise, J. B.; Leinenweber, K.; Weidner, D. J.; Tan, K.; Dreele, R. B. Von. Pressure-
2 Induced H Bonding; Neutron Diffraction Study of Brucite, $\text{Mg}(\text{OH})_2$, to 9.3 GPa. *Am.*
3 *Miner.* **1994**, *79*, 193–196.
- 4 (32) Allmann, R.; Jepsen, H. P. Die Struktur Des Hydrotalkits. *N. Jb. Miner. Mh.* **1969**, *1969*,
5 544–551.
- 6 (33) Arakcheeva, A.V. Pushcharovskii, D.Yu. Rastsvetaeva, R. K.; Atencio, D.; Lubman, G.
7 U. Crystal Structure and Comparative Crystal Chemistry of $\text{Al}_2\text{Mg}_4(\text{OH})_{12}(\text{CO}_3)_3\cdot 3\text{H}_2\text{O}$, a
8 New Mineral from the Hydrotalcite-Manasseite Group. *Crystallogr. Rep.* **1996**, *41*, 972–
9 981.
- 10 (34) Besserguenev, A. V; Fogg, A. M.; Francis, R. J.; Price, S. J.; O'Hare, D.; Isupov, V. P.;
11 Tolochko, B. P. Synthesis and Structure of the Gibbsite Intercalation Compounds
12 $[\text{LiAl}_2(\text{OH})_6]\text{X}$ {X = Cl, Br, NO_3 } and $[\text{LiAl}_2(\text{OH})_6]\text{Cl}\cdot\text{H}_2\text{O}$ Using Synchrotron X-Ray
13 and Neutron Powder Diffraction. *Chem. Mater.* **1997**, *9*, 241–247.
- 14 (35) Palmer, D. C. CrystalMaker. **2014**, CrystalMaker Software Ltd, Begbroke, Oxfordshire,.
- 15 (36) Hudson, M. J.; Carlino, S.; Apperley, D. C. Thermal Conversion of a Layered (Mg/Al)
16 Double Hydroxide to the Oxide. *J. Mater. Chem.* **1995**, *5*, 323–329.
- 17 (37) Yang, W.; Kim, Y.; Liu, P. K. T.; Sahimi, M.; Tsotsis, T. T. A Study by in Situ
18 Techniques of the Thermal Evolution of the Structure of a Mg–Al– CO_3 Layered Double
19 Hydroxide. *Chem. Eng. Sci.* **2002**, *57*, 2945–2953.
- 20 (38) Valente, J. S.; Rodriguez-Gattorno, G.; Valle-Orta, M.; Torres-Garcia, E. Thermal
21 Decomposition Kinetics of MgAl Layered Double Hydroxides. *Mater. Chem. Phys.* **2012**,

133, 621–629.

(39) Gazzano, M.; Kagunya, W.; Matteuzzi, D.; Vaccari, A. Neutron Diffraction Studies of Polycrystalline Ni/Mg/Al Mixed Oxides Obtained from Hydrotalcite-like Precursors. *J. Phys. Chem. B* **1997**, *101*, 4514–4519.

(40) Leont'eva, N. N.; Cherepanova, S. V.; Drozdov, V. A. Thermal Decomposition of Layered Double Hydroxides Mg-Al, Ni-Al, Mg-Ga: Structural Features of Hydroxide, Dehydrated, and Oxide Phases. *J. Struct. Chem.* **2014**, *55*, 1326–1341.

(41) Rascón, F.; Wischert, R.; Copéret, C. Molecular Nature of Support Effects in Single-Site Heterogeneous Catalysts: Silica vs. Alumina. *Chem. Sci.* **2011**, *2*, 1449–1456.

(42) Bellotto, M.; Rebours, B.; Clause, O.; Lynch, J.; Bazin, D.; Elkaïm, E. Hydrotalcite Decomposition Mechanism: A Clue to the Structure and Reactivity of Spinel-like Mixed Oxides. *J. Phys. Chem.* **1996**, *100*, 8535–8542.

(43) Thommes, M.; Kaneko, K.; Neimark, A. V.; Olivier, J. P.; Rodriguez-reinoso, F.; Rouquerol, J.; Sing, K. S. W. Physisorption of Gases, with Special Reference to the Evaluation of Surface Area and Pore Size Distribution (IUPAC Technical Report). *Pure Appl. Chem.* **2015**, *87*, 1051–1069.

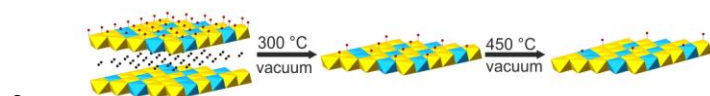
(44) Wang, Q.; Gao, Y.; Luo, J.; Zhong, Z.; Borgna, A.; Guo, Z.; O'Hare, D. Synthesis of Nano-Sized Spherical Mg₃Al–CO₃ Layered Double Hydroxide as a High-Temperature CO₂ Adsorbent. *RSC Adv.* **2013**, *3*, 3414–3420.

(45) Zhuravlev, L. T. The Surface Chemistry of Amorphous Silica. Zhuravlev Model. *Colloids Surf., A* **2000**, *173*, 1–38.

- 1 (46) Zhuravlev, L. T. Concentration of Hydroxyl Groups on the Surface of Amorphous Silicas.
2 *Langmuir* **1987**, *3*, 316–318.
- 3 (47) Zhuravlev, L. T.; Potapov, V. V. Density of Silanol Groups on the Surface of Silica
4 Precipitated from a Hydrothermal Solution. *Russ. J. Phys. Chem.* **2006**, *80*, 1119–1128.
- 5 (48) Davydov, V. Y.; Kiselev, A. V.; Zhuravlev, L. T. Study of the Surface and Bulk Hydroxyl
6 Groups of Silica by Infra-Red Spectra and D₂O-Exchange. *Trans. Faraday Soc.* **1964**, *60*,
7 2254–2264.
- 8 (49) Mueller, R.; Kammler, H. K.; Wegner, K.; Pratsinis, S. E. OH Surface Density of SiO₂
9 and TiO₂ by Thermogravimetric Analysis. *Langmuir* **2003**, *19*, 160–165.
- 10 (50) Lelli, M.; Gajan, D.; Lesage, A.; Caporini, M. A.; Vitzthum, V.; Miéville, P.; Héroguel,
11 F.; Rascón, F.; Roussey, A.; Thieuleux, C.; et al. Fast Characterization of Functionalized
12 Silica Materials by Silicon-29 Surface-Enhanced NMR Spectroscopy Using Dynamic
13 Nuclear Polarization. *J. Am. Chem. Soc.* **2011**, *133*, 2104–2107.
- 14 (51) Fajdala, K. L.; Tilley, T. D. An Efficient, Single-Source Molecular Precursor to
15 Silicoaluminophosphates. *J. Am. Chem. Soc.* **2001**, *123*, 10133–10134.
- 16 (52) Fripiat, J. J.; Uytterhoeven, J. Hydroxyl Content in Silica gel “Aerosil.” *J. Phys. Chem.*
17 **1962**, *66*, 800–805.
- 18 (53) Sato, M.; Kanbayashi, T.; Kobayashi, N.; Shima, Y. Hydroxyl Groups on Silica, Alumina,
19 and Silica-Alumina Catalysts. *J. Catal.* **1967**, *7*, 342–351.
- 20 (54) Itoh, H.; Utamapanya, S.; Stark, J. V.; Klabunde, K. J.; Schlup, J. R. Nanoscale Metal
21 Oxide Particles as Chemical Reagents. Intrinsic Effects of Particle Size on Hydroxyl

- 1 Content and on Reactivity and Acid/base Properties of Ultrafine Magnesium Oxide.
2 *Chem. Mater.* **1993**, *5*, 71–77.
- 3 (55) Van Grieken, R.; Carrero, A.; Suarez, I.; Paredes, B. Ethylene Polymerization over
4 Supported MAO/(*n*BuCp)₂ZrCl₂ Catalysts: Influence of Support Properties. *Eur. Polym. J.*
5 **2007**, *43*, 1267–1277.
- 6
- 7

1 For Table of Contents Only



3 Thermal treatment of layered double hydroxides under vacuum allows for control of the surface
4 hydroxyl concentration. The resulting LDH structures have been spectroscopically characterized
5 and the degree of remaining hydroxyl functionality determined.